SUPPORTING INFORMATION

Templating Effect of Different Low Miller Index Gold Surfaces on the Bottom-Up Growth of Graphene Nanoribbons

Francesco De Boni,[†] Gabriel Merlin,[†] Francesco Sedona*,[†] Stefano Casalini,[†] Mir Masoud Seyyed Fakhrabadi[‡], and Mauro Sambi[†,#]

[†]Dipartimento di Scienze Chimiche, Università degli Studi di Padova, Via Marzolo 1, 35131 Padova, Italy
[‡]School of Mechanical Engineering, College of Engineering, University of Tehran, North Karar Ave, 55555 Tehran, Iran.
[#]Consorzio INSTM, Unità di Ricerca di Padova,35131 Padova, Italy

* Corresponding author: francesco.sedona@unipd.it

1. Au(100) surface: preparation and characterization

The Au(100) surface was cleaned with several cycles of sputtering with Ar^+ ions at an energy of 1000 eV for 1 hour at 500°C, followed by annealing at 550°C for about 30 minutes. The quality of the surface was monitored by means of STM and LEED, until we obtained an ordered and clean surface. A 20×20nm^2 image of the Au(100) surface is reported in Figure S1, with an example of a line profile. The measured distance between the rows, which are oriented along two symmetry-equivalent domains, is $d_1 = (14.6 \pm 0.5)$ Å, in good agreement with the shorter side of the theoretical (5×20) cell of the reconstruction. The corrugation is quite low as expected, in the order of 0.7 Å at maximum.[1,2] A model of the (5×20) surface reconstruction is represented in Figure S1c.

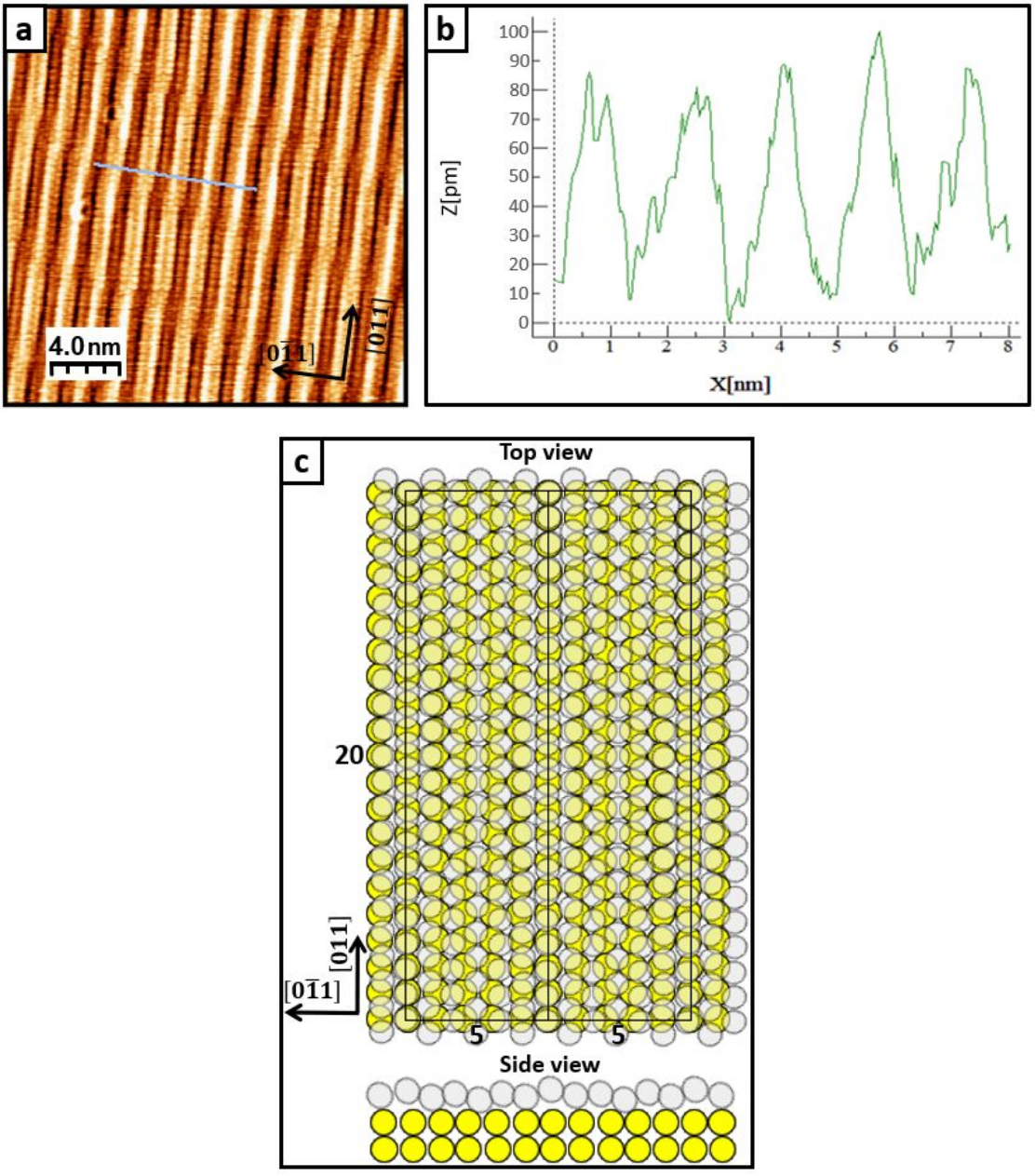

Figure S1 – (a) STM image of the clean Au(100) surface (I = 5.7 nA, V = 0.6 V). (b) Line profile of the surface along the blue line in (a). (c) Top and side view of a model representing the (5×20) reconstruction of the Au(100) surface: the yellow atoms belong to the bulk square lattice, while the grey atoms belong to the quasi-hexagonal topmost layer.

Figure S2 shows the Low Energy Electron Diffraction (LEED) pattern of clean Au(100). Its features are very similar to those reported in the literature, in particular for the presence of double spots, which can be explained by assuming a more complex periodicity than the (5×20) reconstruction.[3]

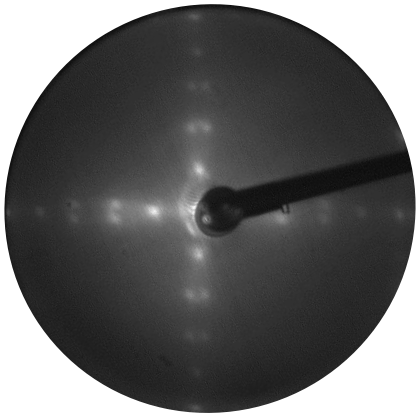

Figure S2 – LEED pattern of clean Au(100) (39 eV).

2. Au(110) surface: preparation and characterization

The surface was cleaned with several cycles of sputtering with Ar^+ ions at an energy of 1000 eV for 1 hour at a temperature of 410°C, followed by annealing at 480°C for 30 minutes. Figure S3 reports a 20×20nm^2 image of the clean surface with an example of a line profile.

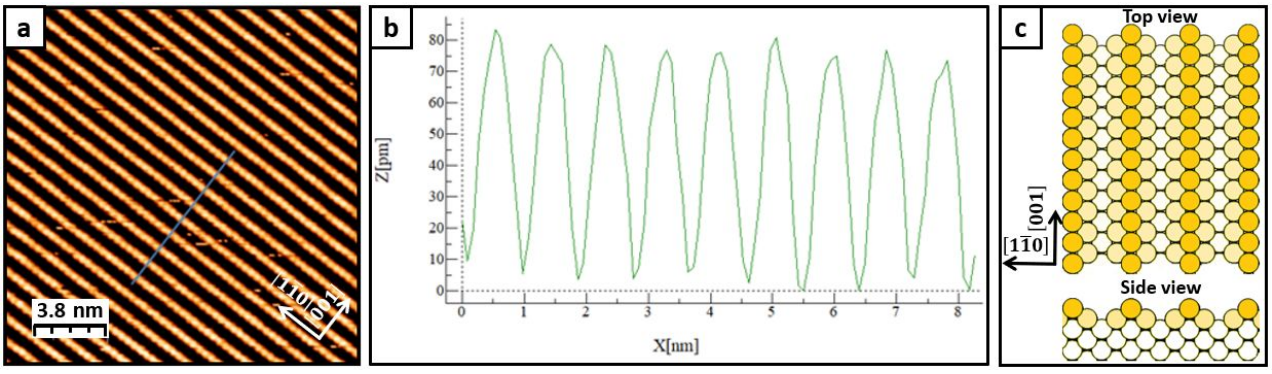

Figure S3 – (a) STM image of the clean Au(110) surface (I = 0.5 nA, V = 0.9 V). (b) Line profile of the surface along the blue line in (a). (c) Top and side view of a model showing the (2×1) reconstruction of the Au(110) surface: different yellow gradations highlight rows of Au atoms at different heights on the surface.

The measured distance between the rows is $d_2 = (8.2 \pm 0.3)$ Å, in very good agreement with the longer side of the (2×1) cell of the "missing row" reconstruction.[4,5] The corrugation is on average 0.9 Å, higher than on Au(100). A model of the (2×1) reconstruction is shown in Figure S3c. The (2×1) reconstruction is also confirmed by the LEED pattern shown in Figure S4.

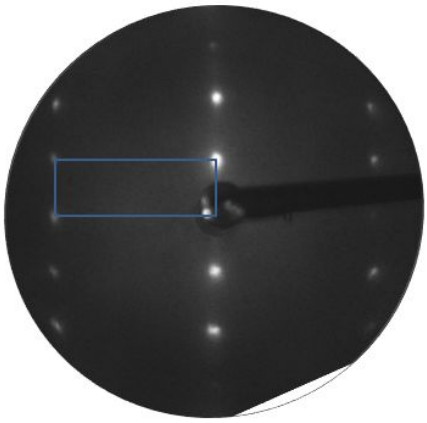

Figure S4 – LEED pattern of the clean Au(110) surface (51 eV); the unit cell is highlighted in blue.

3. Au(111) surface: preparation and characterization

We performed the synthesis of GNRs from DBTP on the Au(111) single crystal surface in the same experimental conditions of the syntheses on Au(100) and Au(110) in order to have a direct comparison between the three experiments. The surface was cleaned with cycles of sputtering with Ar^+ ions at an energy of 1500 eV for 1 hour at a temperature of 410°C, followed by annealing at 480°C for 30 minutes. Figure S5 reports a 130×130nm^2 image of the clean surface, showing the typical "herringbone" reconstruction,[6-8] with an example of a line profile (corrugation of 0.25 Å at maximum).

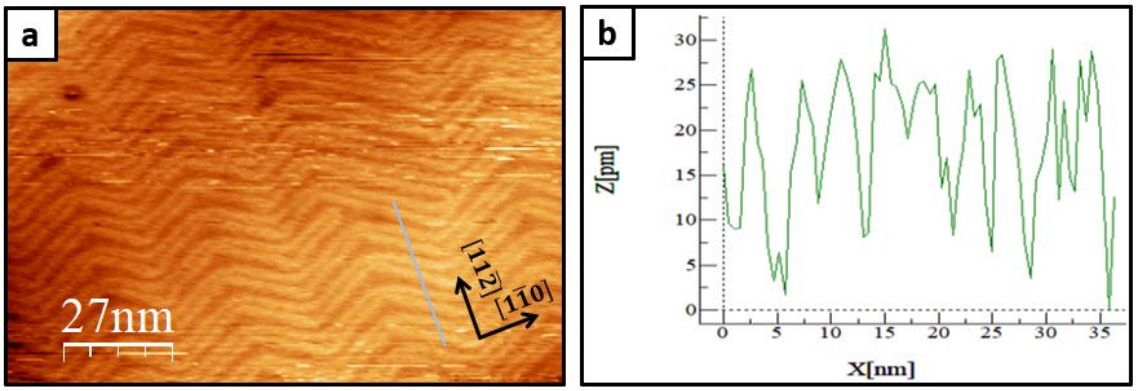

Figure S5 – (a) STM image of the clean Au(111) surface (I = 1.2 nA, V = 1.1 V). (b) Line profile of the surface along the blue line in (a).

4. XPS fitting parameters: additional details

X-ray Photoelectron Spectroscopy (XPS) spectra were fitted with the XPSPeak41 software.[9] For each C 1s peak, we initially performed the fit by fixing the binding energy (BE) and the percentage area of the different components at the expected values (from the literature). We also fixed full-width-at-half-maximum (FWHM) and lineshape (Voigt function), in term of percentage of Lorentzian and Gaussian components, at plausible values (0.7-0.9 eV range for FWHM, 30-70% range for the Lorentzian component in the lineshape).

Subsequently, we let both BE and percentage area free to vary and carried out the fit again, maintaining the other two parameters fixed. The final result was evaluated by looking at the χ^2 parameter: if it was far from 1, which is the correct value for a good simulation, all the parameters of the peak were tuned and the fit repeated.

Tables S1, S2, and S3 summarize the positions (BE) and the relative areas of the different C 1s components for each growth step on Au(100), Au(110), and Au(111), respectively.

Table S1 –XPS peak positions (binding energy, BE, measured in eV) of the different C 1s components for each growth step on Au(100) and the corresponding amount of each component as a percentage of the total peak area.

	Au(100)							
Bonds	**Deposition RT**		**Annealing 200°C**		**Annealing 280°C**		**Annealing 480°C**	
	BE [eV]	Area	BE [eV]	Area	BE [eV]	Area	BE [eV]	Area
C-H	284.2	66.4%	284.0	66.2%	284.2	66.1%	284.1	35.5%
C-C	284.5	22.3%	284.4	33.8%	284.5	33.9%	284.4	64.5%
C-Br	285.1	11.3%						

Table S2 – XPS peak positions (binding energy, BE, measured in eV) of the different C 1s components for each growth step on Au(110) and the corresponding amount of each component as a percentage of the total peak area.

	Au(110)							
Bonds	**Deposition RT**		**Annealing 170°C**		**Annealing 280°C**		**Annealing 360°C**	
	BE [eV]	Area	BE [eV]	Area	BE [eV]	Area	BE [eV]	Area
C-H	284.3	66.9%	284.2	66.8%	284.2	66.4%	284.1	21.1%
C-C	284.6	22.4%	284.5	33.2%	284.6	33.6%	284.3	43.9%
C-Br	285.1	10.7%						
$C_{defective}$							283.7	35.0%

Table S3 – XPS peak positions (binding energy, BE, measured in eV) of the different C components for each growth step on Au(111) and the corresponding amount of each component as a percentage of the total peak area.

	Au(111)							
Bonds	**Deposition RT**		**Annealing 200°C**		**Annealing 250°C**		**Annealing 380°C**	
	BE [eV]	Area	BE [eV]	Area	BE [eV]	Area	BE [eV]	Area
C-H	284.1	66.8%	283.8	66.1%	284.0	66.2%	283.8	26.6%
C-C	284.5	22.1%	284.1	33.9%	284.3	33.8%	284.1	73.4%
C-Br	285.1	11.1%						

Concerning the BE values of C 1s peaks reported in Figure 9 of the main paper, we performed a one-component fit of each peak without imposing any constraint, and we obtained the BE value from the fitted peak maximum. We associated uncertainty to such determination by considering the BE interval in which the y-value of the peak (measured in arbitrary units) decreases by 0.5% at maximum. In this way, for example, the highest uncertainty was obtained for C 1s peaks related to the RT deposition of DBTP, because they have the greatest FWHM owing to the presence of a high BE component (C-Br).

5. Additional details about the synthesis of GNRs on Au(100): different domains of PPP wires

After the annealing at 200°C, poly-*p*-phenylene (PPP) wires are organized in different domains both parallel and forming various angles with respect to the surface reconstruction (see main paper). Figure S6a reports a magnification of the surface where the different domains are clearly visible. Moreover, each domain is characterized by a specific average lateral distance between PPP wires, i.e. (1.4 ± 0.2) nm for the domains along the reconstruction and (1.1 ± 0.2) nm for the other ones (see line profiles in Figures S6b,c).

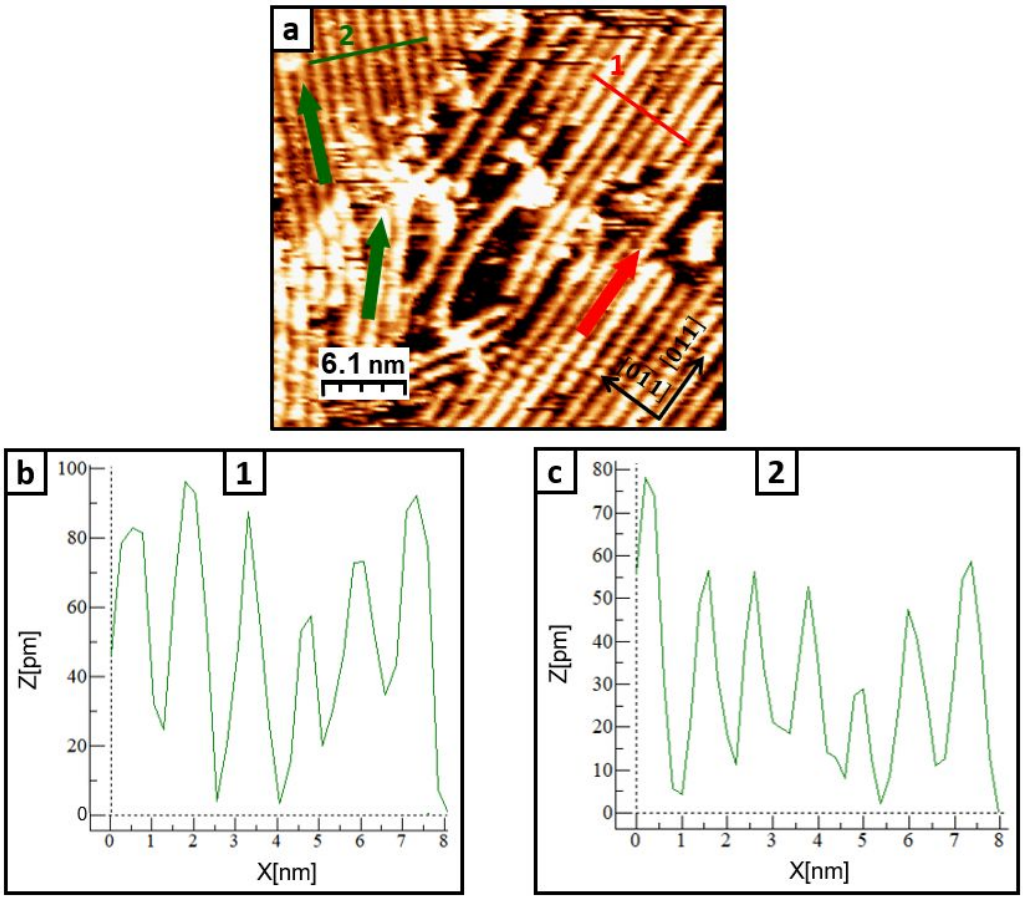

Figure S6 – (a) STM image of the Au(100) surface after annealing at 200°C, showing the presence of PPP domains both parallel (red arrow) and forming various angles (green arrows) compared to the surface reconstruction (I = 0.5 nA, V = -1.1 V). (b) Line profile of the surface along the red line (1) in (a), representative of the domains parallel to the reconstruction. (c) Line profile of the surface along the green line (2) in (a), representative of the domains forming various angles with the reconstruction.

6. Additional details about the synthesis of GNRs on Au(110): STM images and LEED patterns

The different reconstructions of Au(110) during the synthesis of GNRs[10,11] are confirmed also by LEED patterns (Figure S7), unlike the synthesis performed on Au(100). After the room temperature (RT) deposition of the 4,4”-dibromo-*p*-terphenyl (DBTP) molecules, the Au(110) surface arranges in a (5×1) reconstruction, in which the separation between the rows along the $[1\bar{1}0]$ direction is 2.5 times larger than in the pristine (2×1) “missing row” reconstruction of clean Au(110). This new reconstruction is confirmed both by LEED (with a LEEDpat[12] simulation partially superimposed to Figure S7a) and STM (Figure S8). The spots present in the LEED pattern are stretched along the [001] direction, probably for the coexistence of other surface reconstructions with different periodicity.

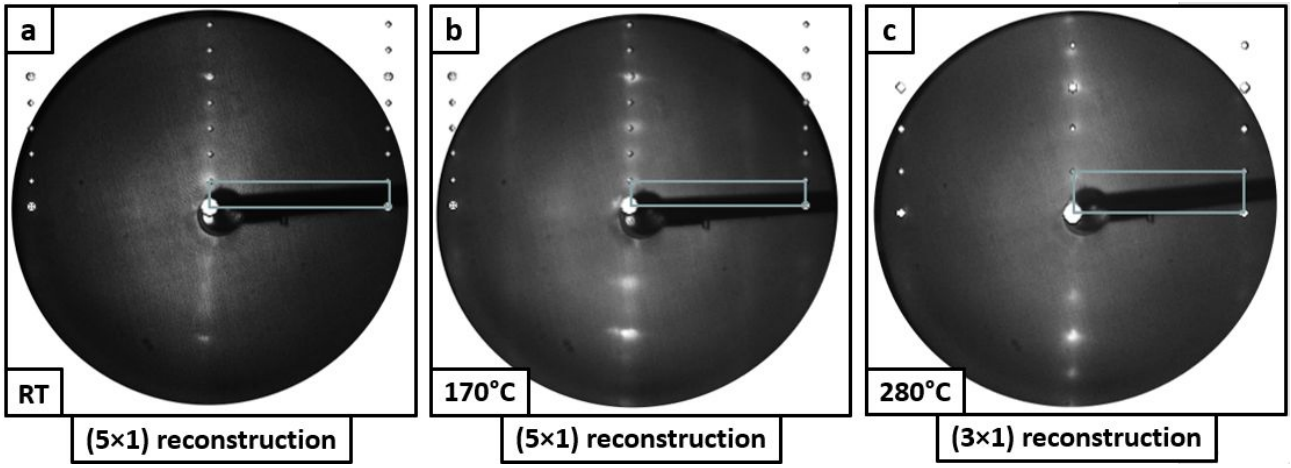

Figure S7 – Au(110) surface LEED pattern with partially superimposed LEEDpat simulation after (a) RT deposition of DBTP molecules (44 eV), (b) annealing at 170°C (46 eV), and (c) annealing at 280°C (51 eV). The corresponding surface reconstruction is specified below each LEED pattern.

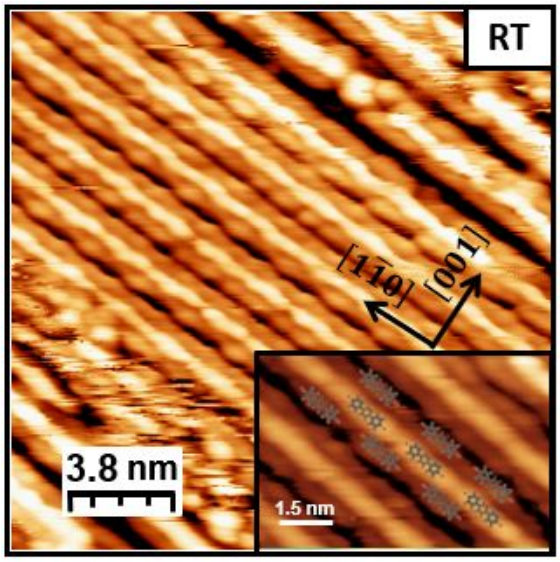

Figure S8 – STM image of the Au(110) surface after RT deposition of DBTP (I = 1 nA, V = -1.1 V). In the bottom inset a magnification of the image with a ball and stick model of DBTP molecules is shown.

A tentative model of DBTP self-assembly on the surface is reported in Figure S9.

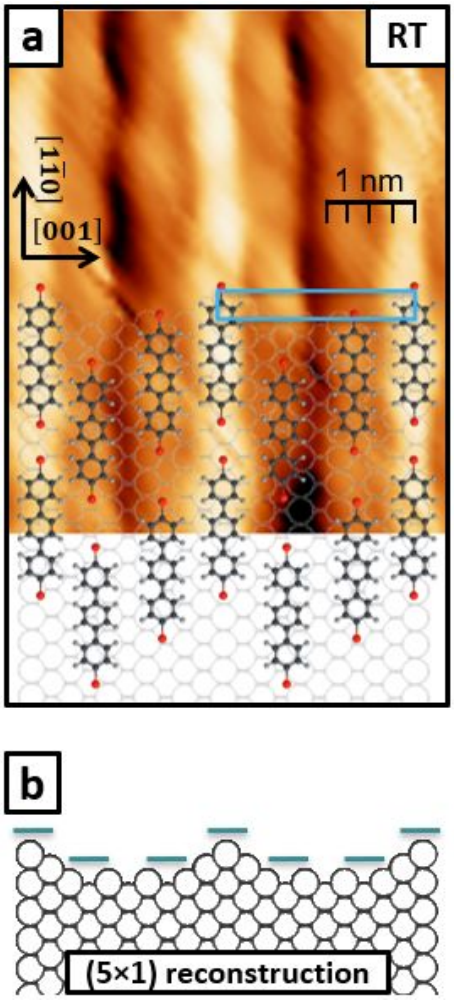

Figure S9 – Top (a) and lateral (b) representations of a possible structure for the Au(110) surface/overlayer system after RT deposition of DBTP. In (a) the model is superimposed to a magnification of the main image of Figure S8. The unit cell of the (5×1) reconstruction is shown in light blue. Its area is 2.874×20.325 Å^2.

Still brominated DBTP molecules (as confirmed by XPS spectra, see main paper) adsorb along the rows both in the valleys and on the ridges of the reconstruction, in a staggered arrangement with respect to each other. The presence of the molecules also on the crests of the reconstruction can be assessed by the contrast difference in STM images.

The rearrangement of the Au(110) surface in presence of adsorbate is well known: a similar situation has been observed for 4,4''-diamino-*p*-terphenyl (DAT), which leads to a (5×1) reconstruction of Au(110) as well.[13] However, even if DAT is structurally very similar to DBTP (it has two amino groups in place of the two bromine atoms), DAT molecules initially settle down perpendicularly to Au(110) channels, i.e. along the [001] direction.

The organization of DBTP molecules after deposition on Au(110) is quite similar to the one observed on Au(111),[14] as shown in Figure S10. In particular, after slight annealing at 50°C, the molecules organize in a staggered configuration along the $[1\bar{1}0]$ direction.

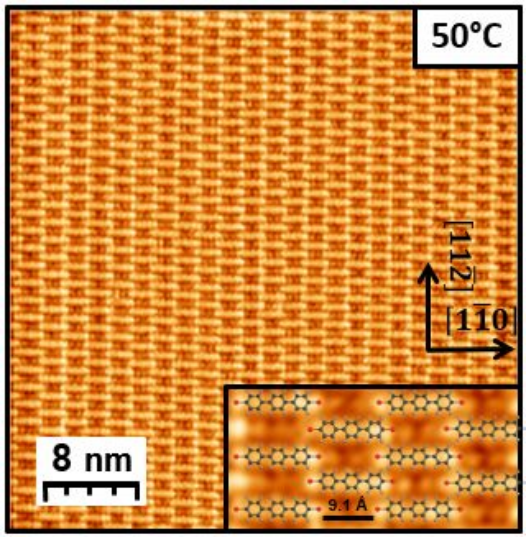

Figure S10 – Self-assembly of DBTP molecules on Au(111). The molecules modify their self-assembly pattern after an annealing at about 50°C, passing form a herringbone-like structure to a configuration more similar to the one observed on Au(110) (I = 4.2 nA; V = -1.5 V). In the bottom inset a magnification of the image with a ball and stick model of DBTP molecules is shown.

The annealing at 170°C promotes the formation of PPP wires along the $[1\bar{1}0]$ direction and the Au(110) surface is observed to maintain a (5×1) reconstruction, which is confirmed by the LEED pattern (Figure S7b). PPP wires stay in pairs within each reconstruction channel and are separated by bromine atoms, producing a very high degree of long-range order (see main paper).

Finally, after the annealing at 280°C that causes the desorption of bromine atoms, the (5×1) reconstruction evolves to a (3×1) motif, in which troughs between the rows are narrower. As a consequence, only one PPP wire per trough along the $[1\bar{1}0]$ direction is present, but the overall long-range order is still high (see main paper). The (3×1) reconstruction is confirmed by the corresponding LEED pattern (Figure S7c).

After this stage, we did not check the surface by LEED because of the increasing disorder within the overlayer.

7. STM images of Br atoms adsorbed between PPP wires on Au(111)

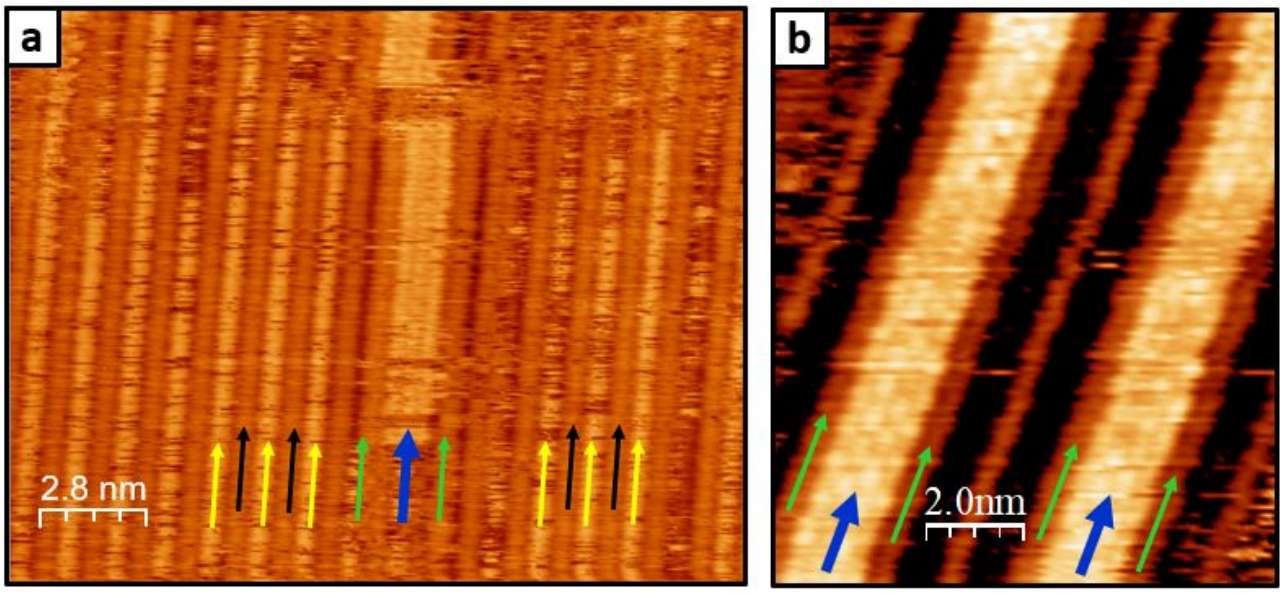

Figure S11 – STM images of the Au(111) surface after annealing at 130°C. In (a) "fuzzy" bright lines (yellow arrows) between regularly spaced PPP wires (black arrows) are visible; moreover, the presence of two more distant wires (green arrows) is also evident, and the space between them is indicated by a blue arrow (I = 8.1 nA; V = 0.3 V). In (b) a magnification of the area between two more distant PPP wires (green arrows) is reported, showing a peculiar hexagonal packing (blue arrows) (I = 8.5 nA; V = -0.5 V).

After the annealing at 130°C, we observe that PPP wires are regularly spaced in some parts of the Au(111) surface, as visible in Figure S11a: in this case, between the wires (black arrows) there are "fuzzy" bright lines that seem to act as spacers (yellow arrows). The STM aspect of these spacers indicates high mobility along the row between two wires. Occasionally, two PPP wires (indicated by the green arrows) are more spaced: in such a situation, the fuzzy lines become more stable and an ordered phase with a hexagonal packing can

be observed (blue arrows in Figures S11a and S11b). This phase is probably due to the presence of Br atoms chemisorbed on the Au surface after the de-halogenation process of DBTP molecules. Hence, Br atoms act as mobile spacers between ordered PPP wires; besides, they can also form more stable islands,[15] so that in these areas of the surface the wires are more spaced.

8. References

[1] Pieczyrak, B.; Trembulowicz, A.; Antczak, G.; Jurczyszyn, L. Nature of Monovacancies on Quasi-Hexagonal Structure of Reconstructed Au(100) Surface. *Applied Surf. Sci.* **2017**, *407*, 345—352.

[2] Havu, P.; Blum, V.; Havu, V.; Rinke, P.; Scheffler, M. Large-Scale Surface Reconstruction Energetics of Pt(100) and Au(100) by All-Electron Density Functional Theory. *Phys. Rev. B* **2010**, *82*, 161418(R).

[3] Van Hove M.A.; Koestner, R.J.; Stair, P.C.; Bibérian, J.P.; Kesmodel, L.L.; Bartos, I.; Somorjai, G.A. The Surface Reconstructions of the (100) Crystal Faces of Iridium, Platinum and Gold: II. Structural Determination by LEED Intensity Analysis. *Surf. Sci.* **1981**, *103* (1), 218—238.

[4] Kolasinski, K.W. *Surface Science: Foundations of Catalysis and Nanoscience*, *4th Ed.*; Wiley: Hoboken, New Jersey, 2020**.**

[5] Somorjai, G.A.; Li, Y. *Introduction to Surface Chemistry and Catalysis*, *2nd Ed.*; Wiley: Hoboken, New Jersey, 2010**.**

[6] Narasimhan, S.; Vanderbilt, D. Elastic Stress Domains and the Herringbone Reconstruction on Au(111). *Phys. Rev. Lett.* **1992**, *69* (10), 1564—1567.

[7] Barth, J.V.; Brune, H.; Ertl, G.; Behm, R.J. Scanning Tunneling Microscopy Observations on the Reconstructed Au(111) Surface: Atomic Structure, Long-Range Superstructure, Rotational Domains, and Surface Defects. *Phys. Rev. B* **1990**, *42* (15), 9307—9318.

[8] Repain, V.; Berroir, J.M.; Rousset, S.; Lecoeur, J. Interaction Between Steps and Reconstruction on Au(111). *Europhys. Lett.* **1999**, *47*, 435.

[9] XPSPeak 4.1, https://xpspeak.software.informer.com/4.1/

[10] Massimi, L.; Ourdjini, O.; Lafferentz, L.; Koch, M.; Grill, L.; Cavaliere, E.; Gavioli, L.; Cardoso, C.; Prezzi, D.; Molinari, E.; Ferretti, A.; Mariani, C.; Betti, M.G. Surface Assisted Reaction toward Formation of Graphene Nanoribbons on Au(110) Surface. *J. Phys. Chem. C* **2015**, *119* (5), 2427—2437.

[11] Della Pia, A.; Avvisati, G.; Ourdjini, O.; Cardoso, C.; Varsano, D.; Prezzi, D.; Ferretti, A.; Mariani, C.; Betti, M.G. Electronic Structure Evolution during the Growth of Graphene Nanoribbons on Au(110). *J. Phys. Chem. C* **2016**, *120* (13), 7323—7331.

[12] LEEDpat 4.2, FHI Berlin, http://www.fhi-berlin.mpg.de/KHsoftware/LEEDpat/

[13] Ren, J.; Bao, D.-L.; Dong, L.; Gao, L.; Wu, R.; Yan, L.; Wang, A.; Yan, J.; Wang, Y.; Du, S.-X.; Huan, Q.; Gao, H.-J. Thermo-Controllable Self-Assembled Structures of Single-Layer 4,4''-diamino-p-terphenyl Molecules on Au(110). *Chin. Phys. B* **2017**, *26* (8), 086801.

[14] Basagni, A.; Sedona, F.; Pignedoli, C.A.; Cattelan, M.; Nicolas, L.; Casarin, M.; Sambi, M. Molecules-Oligomers-Nanowires-Graphene Nanoribbons: A Bottom-Up Stepwise On-Surface Covalent Synthesis Preserving Long-Range Order. *J. Am. Chem. Soc*. **2015**, *137* (5), 1802—1808.

[15] Nanayakkara, S. U.; Sykes, E. C. H.; Fernández-Torres, L. C.; Blake, M. M.; Weiss, P. S. Long-Range Electronic Interactions at a High Temperature: Bromine Adatom Islands on Cu(111). *Phys. Rev. Lett.* **2007**, *98*, 206108.